Crystallization study and hyperfine characterization of a Sn-O thin film with ^{181}Ta

M. S. Moreno, J. Desimoni, A. G. Bibiloni, M. Rentería, and C. P. Massolo
Departamento de Fisica, Facultad de Ciencias Exactas, Universidad Nacional de La Plata, Casilla de Correo No. 67, 1900 La Plata, Argentina

K. Freitag
Institut für Strahlen- und Kernphysik, der Universität Bonn, Nussallee 14-16, 5300 Bonn, Germany
(Received 15 May 1990; revised manuscript received 10 September 1990)

We present here a study, through perturbed angular correlation (PAC), of a ^{181}Ta-implanted Sn-O thin film prepared by thermal evaporation of tin in a 10^{-3}-Torr oxygen atmosphere. The film, as prepared, was characterized by conversion-electron Mössbauer spectroscopy (CEMS). These data revealed the two oxidation states, namely, 2+ and 4+, for ^{119}Sn. The film evolution was monitored by PAC at room temperature (RT) after each step of two series of thermal annealings performed on the sample. The first series was carried out in Ar in the temperature range 473–773 K while the second was carried out on the same film in air in the temperature range 473–1373 K. Complementary CEMS studies were also performed after following the same annealing steps on a similar film. These results clearly show the evolution of the sample to a 4+ oxidation state, corresponding to SnO_2, and a total crystallization for annealing at 1373 K. This fact allows a hyperfine characterization of ^{181}Ta impurities substitutionally replacing tin in the perfect SnO_2 lattice, in the PAC measurement following the annealing at 1373 K. It is worthwhile mentioning that in the CEMS measurements, in the range 473–573 K of the first series, the parameters of the 2+ state correspond to crystalline SnO; as a consequence, a tentative hyperfine characterization by PAC of SnO was also possible. Furthermore, point-charge-model calculations were performed and a systematic survey of the antishielding factor β of ^{181}Ta in different oxides is given.

I. INTRODUCTION

Thin films of transparent oxides such as In_2O_3, SnO_2, and ITO (In_2O_3:Sn) are increasingly used in devices on which transparent conductor coatings are needed. Among them, tin oxide films are of particular importance since they find applications in solar cells, gas-sensing elements, and electronic components. Both amorphous and crystalline films are used for this purpose. Optical and electrical properties are found to depend on the crystalline state of the films—hence the special interest in studying all stages in the amorphous-crystalline transition.

In the past few years, the perturbed-angular-correlation (PAC) technique has been increasingly applied to study semiconductor oxides (see Refs. 1–4 and references cited therein). The single-atom counting of this technique, in combination with the highly localized sensitivity (due to the r^{-3} dependence of the quadrupole interaction) allows a detailed investigation of both structural and electronic characteristics. Therefore, PAC measurements are ideal tools to track the evolution of a film from the amorphous to the crystalline state since the different coexisting phases can be separately characterized.

Recently,[5] PAC measurements were performed on SnO_2 films prepared by thermal evaporation using diffused $^{111}In \xrightarrow{EC} {}^{111}Cd$ as a probe with In undergoing an electron-capture (EC) decay. The aim of the experiment was to obtain a hyperfine characterization of the final product, crystalline SnO_2. Confirming previous results on SnO_2 powder samples,[6] the presence of two hyperfine electric quadrupole interactions has been found, revealing the existence of two different sites for ^{111}Cd in the lattice. From their temperature dependence, they were ascribed to the trapping of a single oxygen vacancy, with different ionization states. This trapping was probably favored by the lower valence of indium compared with that of tin. The hyperfine parameters of the interactions, i.e., the quadrupole coupling constant and asymmetry parameter, were the same in powder samples and crystalline films. Preliminary PAC results on ion-implanted indium in Sn-O thin films[7] show, at room temperature, that after annealing in air at 1023 K, crystalline SnO_2 coexists with other structures and oxidation states. No temperature-dependence studies have been carried out yet in these implanted films. The use of $^{181}Hf^{4+}$ probes, which do not favor vacancy trapping in tin dioxide, and therefore allow the study of a defect-free system, seems to be the next logical step in the study of SnO_2 crystalline films with PAC.

Now, from a general point of view, the problem is the following. Although much work has been done investigating the Sn-O system with use of several experimental techniques, there are still discrepancies concerning the different steps in the evolution from tin plus oxygen to the perfect SnO_2 crystalline structure.

It is well known that tin oxide films obtained by different methods—such as spray, electron-beam eva-

poration, chemical vapor deposition, thermal evaporation, etc.—are amorphous and oxygen defficient (SnO_x, $x<2$). Post-deposition annealing treatments in an oxygen atmosphere or air lead, through mixtures where different intermediate oxides coexist, to the proper crystalline tin dioxide. The occurrence of these stages depends strongly on the sample preparation and sequence of the annealings.

Some insight into the character of amorphicity in Sn-O systems has been presented by Collins *et al.*[8] They prepared SnO_2 films in the following way: Pure metallic tin was evaporated on a cooled aluminum backing in a chamber filled with oxygen at about 1×10^{-3} Torr. These authors found, through Mössbauer spectroscopy, electron micrography, and electron diffraction, that samples evaporated at a low rate were composed of a mixture of SnO and SnO_2, both amorphous. Mössbauer-spectroscopy studies carried out in the temperature range 115–470 K revealed that only amorphous SnO_2 was present at 470 K. They attributed the amorphous character to an elongation of the Sn—O bonds in the axial direction of the crystalline SnO and SnO_2. They suggested that the amorphous Sn-O is composed of units of distorted octahedra with central Sn^{4+} linked by Sn—O bonds, where bridging Sn^{2+} ions lie at the apex of a pyramid.

Feng, Ghosh, and Fishman[9] reported x-ray studies and photovoltaic properties in SnO_2 films, prepared by electron-beam deposition and spraying a mixture of $SnCl_4$ onto a heated silicon substrate. They found that fresh films are composed of a mixture of different phases, while SnO_2 seems to dominate after a 1-h annealing at 573 K in air.

In Ref. 10 the films were prepared by electron-beam evaporation of tin dioxide powder under controlled deposition conditions. X-ray-diffraction analysis revealed that the films deposited onto substrates at temperatures lower than 573 K were amorphous. Different preliminary oxidation states, namely, SnO and Sn_3O_4, were found when the films were annealed at 573 K in an oxygen atmosphere, depending on the deposition temperature. In all cases the final oxide SnO_2 was obtained after annealings at 873 K, but the results indicate that an amorphous fraction of tin oxide still remains.

Tafto, Rajeswaran, and Vanier[11] also studied tin oxide thin films prepared by reactive sputtering. They characterized and studied the local structure in the amorphous SnO_2 through electron-microscopy diffraction and electron-energy-loss spectroscopy, concluding that the local atomic arrangement of the films is nearly the same as in crystalline SnO_2. Therefore, according to their results, the amorphous phase in tin oxide should correspond to a positional disorder, i.e., the atoms are slightly displaced in a random way from their ideal positions.[12]

In summary, the different preparation methods lead to amorphous and oxygen-defficient tin oxide films. Annealing treatments in oxygen or air lead to the proper crystalline tin dioxide through different steps. The amorphous phases, more properly disorderly phases, could correspond to a positional disorder.

We present here the results of PAC experiments on a thermally evaporated tin oxygen film with implanted ^{181}Hf probes. Measurements were carried out at room temperature following an annealing program up to 1373 K. The oxidation states of Sn in the film were monitored by conversion-electron Mössbauer spectroscopy (CEMS) measurements.[13] We have characterized the hyperfine interaction of ^{181}Ta in the different steps of the amorphous-crystalline states of the system.

The significance of point-charge-model (PCM) calculations on semiconductor oxides have become apparent[14–16] after the pioneer work of Bolse, Uhrmacher, and Kesten.[17] Comparison of our results, as well as those of others reported in the literature also using ^{181}Ta as probes, with PCM calculations, is also presented.

II. EXPERIMENT

The films were prepared by thermal evaporation of high-purity metallic tin (99.999% purity) in a vacuum chamber where after air evacuation a flux of pure oxygen was introduced and kept at a pressure of about 2×10^{-3} Torr. The substrate consisted of an optically polished rectangular quartz plate. The estimated thickness of the films was less than 300 nm, and the temperature of the substrate during evaporation was around 300 K.

The $^{181}Hf^{+}$ ions with energies of 150 keV were implanted in the ion accelerator of the Institut für Strahlen- und Kernphysik (ISKP). The total calculated dose was $\leq 8\times10^{13}$ ions/cm^2 ($\simeq 100\ \mu$Ci).

The PAC measurements were carried out after annealings for 1 h at 473, 573, 673, and 773 K in an Ar atmosphere and at 473 and 573 K in air. Three additional annealings were performed in air at 1043 and 1173 K for 2 h and at 1373 K for 1 h.

A conventional two-detector apparatus with CsF scintillators was used on the well-known 133–482-keV γ-γ cascade of ^{181}Ta. The electronic equipment and data-recording apparatus are described elsewhere.[18] Theoretical functions of the form $A_2G_2(t)$ folded with the time resolution curve (full width at half maximum of 0.9 ns) were fitted to the experimental $R(t)$ asymmetry ratio:

$$R(t)=2\frac{N(180°,t)-N(90°,t)}{N(180°,t)+2N(90°,t)}\simeq A_2G_2(t)\ . \tag{1}$$

The assumed perturbation factor was of the form

$$G_2(t)=\sum_i f_i \sum_{n=0}^{3} S_{2n,i}\cos(\omega_{n,i}t)\exp(-\delta_i\omega_{n,i}t)\ , \tag{2}$$

where f_i are the relative fractions of nuclei that experience a given perturbation. The ω_n frequencies are related by $\omega_n=g_n(\eta)\nu_Q$ to the quadrupole coupling constant $\nu_Q=eQV_{zz}/h$. The g_n and S_n coefficients are known functions[19] of the axial-asymmetry parameter $\eta=(V_{xx}-V_{yy})/V_{zz}$. The exponential functions account for a Lorentzian frequency distribution of relative width δ around ω_n.

Mössbauer spectra were recorded in a conventional constant-acceleration spectrometer with backscattering geometry. The electron detector used a mixture of flowing He and methane gas. Calibration was performed against a 6-μm α-Fe absorber. The nonlinearity was fitted with a second-degree polynomial. Isomer shifts are referred to a $CaSnO_3$ absorber. The 5-mCi Ba $^{119m}SnO_3$

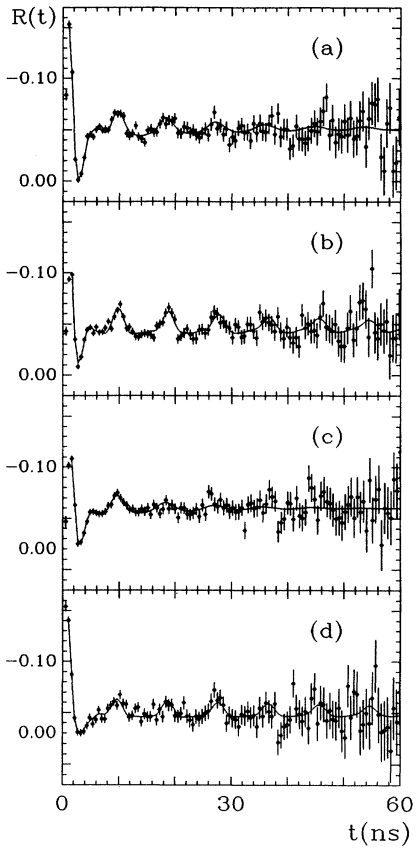

FIG. 1. PAC spectra of ^{181}Hf implanted in a Sn-O film taken at room temperature (RT), after the following series of annealings for 1 h in Ar atmosphere: (a) 473 K, (b) 573 K, (c) 673 K, and (d) 773 K. The solid line correspond to a least-squares fits of Eq. (2) to the data.

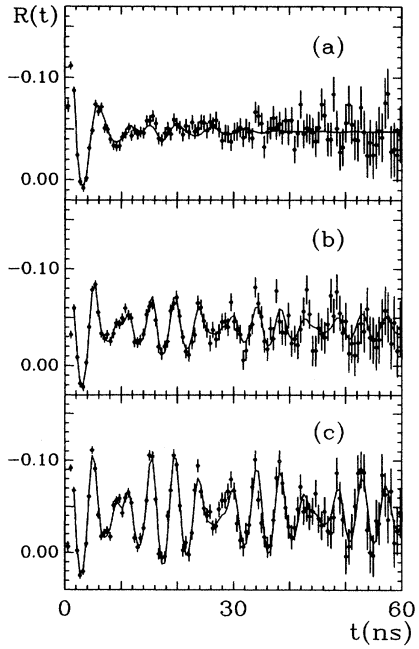

FIG. 2. PAC spectra of ^{181}Hf taken at RT, after the following series of annealings in air: (a) 1043 K, 2 h, (b) 1173 K, 2 h, and (c) 1373 K, 1 h. The solid line correspond to a least-squares fits of Eq. (2) to the data.

source was kept at room temperature and driven in a triangular waveform.

A nonlinear least-squares program with constraints was used to fit the CEMS spectra.

III. RESULTS AND DISCUSSION

A. Data analysis

After implantation, a predetermined annealing program was carried out. Thermal treatments lasting 1 h in the range 473–773 K were performed in an argon atmosphere to remove radiation damage as well as to favor the substitutional accommodation of the probe into a Sn site in the lattice. PAC spectra taken at room temperature immediately after each treatment are shown in Fig. 1. Afterwards, another series of annealings in the range 473–1373 K was performed, but this time in air in order to achieve full oxidation of the film. The relevant spectra are shown in Fig. 2. In Tables I and II the results of least-squares fits of Eq. (2) to the data are displayed.

In the first series (see Fig. 1 and Table I), a well-defined interaction, labeled as hfi_{I}, characterized by $\nu_Q = 752$ MHz and $\eta = 0.0$ is superimposed over a broad distribution centered at about 1000 MHz [$(\text{hfi})_{\text{II}}$]. The relative intensities of the two interactions remain constant within errors throughout the whole series.

Measurements performed after the second series of thermal treatments in air show a net intensity evolution of the two present quadrupole interactions. The interaction labeled $(\text{hfi})_{\text{III}}$ in Table II, which after the 1043-K treatment represents half of the total intensity, disappears after annealing at 1373 K in air. The interaction $(\text{hfi})_{\text{IV}}$, characterized by $\nu_Q = 968$ MHz and $\eta = 0.72$, has similar hyperfine parameters to those of $(\text{hfi})_{\text{II}}$ measured after

TABLE I. Results of least-squares fits of Eq. (2) to the data showed in Fig. 1.

Anneal treat.	$(\text{hfi})_{\text{I}}$ f_1 (%)	ν_{Q_1} (MHz)	η_1	δ_1 (%)	$(\text{hfi})_{\text{II}}$ f_2 (%)	ν_{Q_2} (MHz)	η_2	δ_2 (%)
473 K, 1 h	16_4	757_6	$0.0_{1.6}$	7_2	84_{44}	1018_{51}	$0.5_{0.1}$	32_6
573 K, 1 h	12_1	745_6	$0.1_{0.1}$	2_1	88_8	1044_{64}	$0.6_{0.2}$	42_4
673 K, 1 h	17_5	764_{19}	$0.0_{1.0}$	11_3	83_{42}	968_{223}	$0.6_{0.3}$	43_{24}
773 K, 1 h	10_2	745_6	$0.0_{0.2}$	2_1	90_9	993_{127}	$0.2_{0.2}$	53_6

TABLE II. Results of the least-squares fits of Eq. (2) to the data displayed in Fig. 2. The fitted parameters for the measurement at 1173 K are also included.

Anneal. treat.	$(hfi)_{III}$ f_3 (%)	ν_{Q_3} (MHz)	η_3	δ_3 (%)	$(hfi)_{IV}$ f_4 (%)	ν_{Q_4} (MHz)	η_4	δ_4 (%)
1043 K, 2 h	48_{10}	770_{19}	$0.6_{0.0}$	9_2	52_{13}	974_{13}	$0.6_{0.0}$	8_3
1173 K, 2 h	47_{18}	815_{51}	$0.7_{0.1}$	20_7	53_8	974_0	$0.7_{0.0}$	2_0
1373 K, 1 h					100_3	968_0	$0.7_{0.0}$	1_0
					100_4 [a]	965_1 [a]	$0.7_{0.0}$ [a]	1_0 [a]

[a]Measured at 1173 K.

low-temperature annealings in Ar, but with a much narrower frequency distribution. The corresponding fraction increases up to 100% after a 1373-K treatment in air.

In order to obtain additional information to help in the analysis of the PAC data, we performed CEMS measurements on identical samples, after the same sequence of thermal treatments. Typical spectra are shown in Fig. 3. In the temperature range 473–573 K, the CEMS spectra showed the characteristic line of the Sn^{2+} oxidation state, with hyperfine parameters (see Table III) in agreement with those attributed to the crystalline SnO.[8] The hyperfine parameters of the peak associated with the Sn^{4+} oxidation state in Figs. 3(a) and 3(b) do not coincide with the SnO_2 crystalline ones. This interaction should then be ascribed to some evolving configuration. It can also be seen in Fig. 3 and Table III that with increasing annealing temperature in air, the full oxidation of tin has taken place. The final oxidation state Sn^{4+}, reached after 1373 K [see Fig. 3(c)] corresponds to crystalline SnO_2.

The comparison of CEMS and PAC results allows the following assignment for the interactions measured by PAC.

(i) The interaction $(hfi)_I$, the only one well defined at low annealing temperatures ($\delta_1 < 10\%$), can be attributed to ^{181}Ta probes in substitutional tin sites of crystalline SnO. Indeed, in this temperature range, the CEMS results display the presence of crystalline SnO. Unfortunately the recoil-free fraction of tin in such an admixture of oxides is not known. Therefore, no conclusions can be extracted from the fitted fractions in the Mössbauer spectra. For a conclusive assignment of $(hfi)_I$, experiments on SnO powder should be performed.

(ii) The interaction $(hfi)_{II}$, present in the Ar annealing series, might be associated with the 4+ oxidation state in the CEMS spectra. In the CEMS results on the sample annealed above 1043 K in air, tin ions exhibits only its 4+ oxidation state. Therefore, the interactions labeled as $(hfi)_{II}$ and $(hfi)_{III}$ must correspond to some SnO_2 without the perfect octahedral structure. They can include configurations such as those reported by Collins *et al.*[8] and Tafto, Rajeswaran, and Vanier.[11] Nonstoichiometric oxides formed during preparation as well as remaining radiation damage due to ion implantation could also contribute to $(hfi)_{II}$.

The presence of the interaction $(hfi)_{III}$ is consistent with results obtained by Madhusudhana Reddy, Jawalekar, and Chandorkar.[10] Their x-ray spectrogram performed after annealing at 873 K in air shows, in addition to some of the SnO_2 characteristic peaks, an amorphous background.

(iii) Concerning the interaction $(hfi)_{IV}$, which is noticeable after an annealing at 1043 K in air and is unique above 1373 K, it should be attributed to Ta ions at regular cation sites in a SnO_2 crystalline lattice, in agreement with our CEMS results. In effect, after the annealing at 1373 K, the 4+ state has the characteristic parameters of crystalline SnO_2.

As can be seen in Tables I and II, all the interactions evolve to the interaction $(hfi)_{IV}$ corresponding to the total oxidation and crystallization of the sample.

As we mentioned in the Introduction, tin oxide thin film prepared by different methods shows sometimes, in its evolution from SnO to SnO_2, the presence of an intermediate oxide, namely, Sn_3O_4, resulting from the decom-

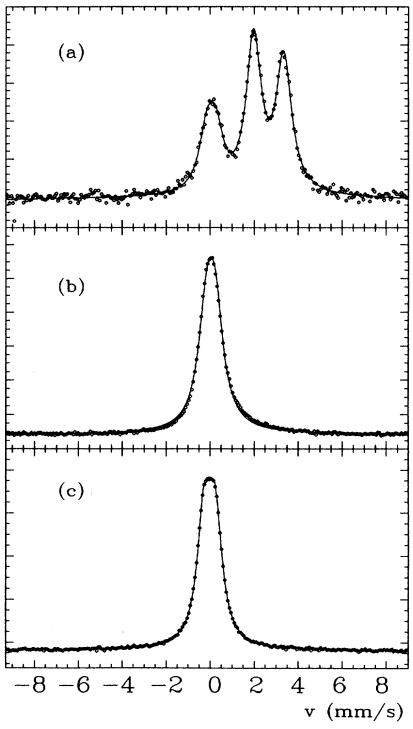

FIG. 3. Typical CEMS spectra at RT taken on a Sn-O film after the same sequence of annealings as in the PAC measurements: (a) 573 K, (b) 1043 K, and (c) 1373 K. The peaks on the right in (a) correspond to the doublet belonging to the Sn^{2+} oxidation state. The other corresponds to the Sn^{4+} oxidation state.

TABLE III. Fitted hyperfine parameters corresponding to the CEMS spectra shown in Fig. 3. Parameters labeled a are those corresponding to SnO_2 and SnO crystalline reported in Ref. 8.

Anneal. treat.	Quadrupole splitting Δ_1 (mm/s)	4+ Isomer shift δ_1 (mm/s)	Linewidth (FWHM) Γ_1 (mm/s)	Quadrupole splitting Δ_2 (mm/s)	2+ Isomer shift δ_2 (mm/s)	Linewidth (FWHM) Γ_2 (mm/s)
573 K, 1 h	0.409_{41}	0.027_{11}	0.837_{57}	1.356_8	2.632_6	0.789_{14}
1043 K, 2 h	0.378_{11}	0.003_2	0.886_{12}			
1373 K, 1 h	0.497_1	0.002_3	0.753_1			
	0.499_{13} [a]	0.004_3 [a]	0.965_{16} [a]	1.36_1 [a]	2.678_3 [a]	0.916_8 [a]

[a]Crystalline data from Ref. 8.

position of SnO. The position of the ions in this lattice is not known yet. The interaction $(hfi)_{II}$, broadly distributed, can include this oxide. Further experiments in progress could clarify the dynamics of the process.

The probe oxidation, that is, the formation of embryos of hafnium oxide, was discarded due to the low width of the frequency distribution of the interaction $(hfi)_{IV}$, which is in contrast to the large distribution which characterizes the embryos of indium oxide.[2] Since the concentration of impurities, ^{181}Hf, is very low ($\simeq 30$ ppm), no macroscopic influence is to be expected. In fact, both films, pure and ^{181}Hf doped, became transparent at the same temperature after annealing at 1043 K. Concerning a possible microscopic influence of the impurity in the crystallization processes, no evidence was found. Before the annealing at 1043 K, the CEMS parameters are compatible with more than one neighborhood for Sn^{4+} ions, which is reflected in the PAC spectra by the existence of two interactions. After annealing above 1373 K, both techniques showed just one interaction, assigned to crystalline SnO_2. Unfortunately, no comparison could be done concerning the intensities of the interactions measured with PAC and CEMS since the recoil-free fractions are unknown in such admixture of oxides.

In order to investigate the temperature dependence of the electric-field gradient (EFG) in the SnO_2 films, we performed a complementary PAC measurement at 1173 K. The resulting spectrum coincides with the one measured at room temperature shown in Fig. 2(c). The constancy of ν_Q with temperature can be due to the s character of the conduction band[20] in SnO_2. The same dependence was found for the EFG of ^{111}Cd in SnO_2 powder.[6] To complete the comparison with the mentioned PAC investigation in SnO_2 powder, we can mention that in the present experiment we did not find any evidence of near-neighbor oxygen vacancy as was found in Ref. 6. This result is consistent with the 4+ valence of ^{181}Hf which should not favor vacancy trapping.

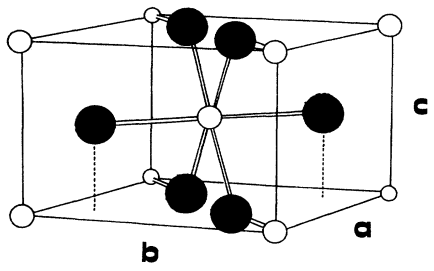

FIG. 4. Sketch showing the way the atoms are placed in the unit cell of SnO_2. Black spheres represent oxygen ions.

B. Calculations

According to the ionic character of both oxides studied, we have performed point-charge-model calculations of EFG's and asymmetry parameters at cation sites in SnO_2 and SnO.

The crystal structure[21] of SnO_2 is of rutile type [$a = 4.7373(1)$ Å, $b = 4.7368(2)$ Å, $c = 3.1862(1)$ Å], where Sn^{4+} is placed in a distorted octahedron, and all Sn-O distances are equal in the basal plane (2.05 Å). The O—Sn—O angles are 78° and 102°, respectively. The Sn-O axial distance in the perpendicular direction to the basal plane is 0.2% longer than those in the base (see Fig. 4). The crystal structure of the SnO is also tetragonal[22] [$a = 3.8029(5)$ Å, $c = 4.8382(8)$ Å]; the tin 2+ ions are at the apex of a square pyramid. This disposition yields a platelike crystallographic morphology for SnO, with Sn-O distances equal to 2.224 Å and angles O—Sn—O of 117.3° (see Fig. 5).

According to our calculations, the predicted asymmetry parameters (for a sphere of 100-Å radius around the probe) are zero and 0.20 for SnO and SnO_2, respectively, and the principal components of the electric-field gradient are nearly the same. The predicted asymmetry parameters are in good agreement for the interaction attributed to SnO, while it does not fit our SnO_2 result. In

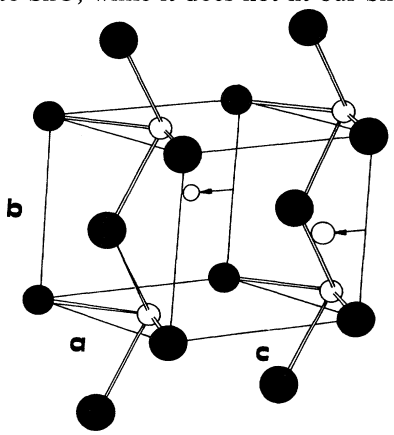

FIG. 5. Perspective drawing of the unit cell of SnO. Black spheres represent the oxygen atoms. The arrows indicate that the tin atoms lay in the face defined by b and c.

this structure the η parameter is very sensitive to slight discrepancies in the atomic coordinates reported by the authors of Refs. 21 and 23. A second discrepancy is found that concerns the EFG, since the PAC results show different coupling constant for the compounds.

Since the cell constants are bigger and the number of atoms per unit cell is smaller for SnO than SnO_2, the SnO crystalline structure is more open than the corresponding to SnO_2. This means that more space is available. This fact should allow a better substitution of the cation ions by ^{181}Hf probes in the case of SnO. On the other hand, it is known that in the crystalline SnO_2 the octahedron is distorted with Sn-O distances smaller than the sum of the individual diameters of the respective ions. The fact that the ionic radius of the probe (^{181}Hf) is bigger than that of Sn (0.81 and 0.71 Å, respectively), as well as the different electronic structures, makes it difficult to predict how the local structure becomes relaxed. Nevertheless, it is worthy to note the fact that a value of $\eta=0.7$ is obtained through a point-charge-model calculation assuming an elongation of just 2.2% in the axis of the octahedra. That value is less than what would be required by the difference in the probe-cation radii, but as was already mentioned, even the O-Sn-O ionic diameter sum is less than the measured distances in the compound. It should be pointed out that the mentioned elongation is not equivalent to the amorphicity suggested by Collins *et al.*[8] because that elongation is a relaxation induced by the probe. Unfortunately, theoretical calculations on this type of lattice impurity-induced relaxation on this system are as yet unavailable.

In order to compare properly the PCM predictions for the EFG and the experimental results, one should take into account the antishielding factor β.

As we mentioned in the Introduction, interesting information can be obtained from comparison of PAC results with simple point-charge-model calculations in ionic compounds. These calculations have been successfully used recently in the analysis of the complicated α-Nb_2O_5 (Ref. 14) PAC spectra and in the determination of the lattice position of oxygen vacancies in reduced MoO_3.[15] In Ref. 16, Bolse *et al.* stated that the antishielding factor β, defined as ν_Q^{expt}/ν_Q^{pc}, where ν_Q^{expt} and ν_Q^{pc} are the experimental and calculated quadrupole coupling constants, respectively, is mostly determined by the nearest-neighbor (*NN*) oxygen coordination, increasing with the number of *NN* oxygen ions.

According to the definition proposed in Ref. 17, β factors in the present case result, $\beta_{SnO}=72.3_{1.5}$ and $\beta_{SnO_2}=99.2_{2.1}$. In agreement with that stated in Ref. 16, the resulting antishielding factor for ^{181}Ta in stannic oxide, with sixfold coordination, is bigger than the one for stannous oxide, with fourfold coordination. We note that the errors in the β values quoted below originate from the lack of precision in the nuclear quadrupole moment $Q(\frac{5}{2})=(+)2.36_5 b$ used in the calculations.[24]

Three more β factors for ^{181}Ta can be calculated from the literature. Using the measured coupling constants for monoclinic and tetragonal zirconium dioxide[25] and

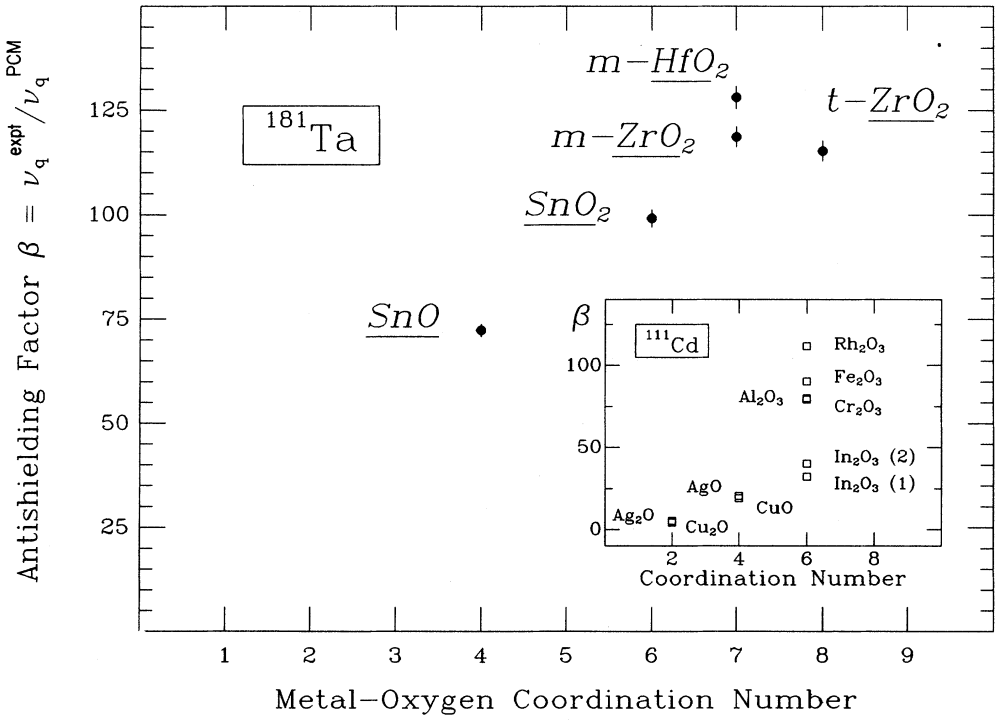

FIG. 6. Antishielding factor β, defined as $\beta=\nu_{zz}^{expt}/\nu_{zz}^{pc}$, as a function of the metal-oxygen coordination number. The ν_{zz}^{expt} corresponds to PAC measurements using ^{181}Ta as probe. Results obtained with ^{111}Cd as probe, obtained from Ref. 16(b), are showed in the inset for comparison.

monoclinic hafnium dioxide,[26] and the crystallographic data taken from Refs. 27–29, respectively, the antishielding factors values $\beta_{m\text{-}ZrO_2}=118.7_{2.5}$, $\beta_{m\text{-}HfO_2}=128.1_{2.7}$, and $\beta_{t\text{-}ZrO_2}=115.3_{2.4}$ are obtained. Their behavior (see Fig. 6) agree with their seven- and eightfold coordination.

Although a dependence on the coordination number for the case of ^{181}Ta becomes also apparent, before any conclusion can be extracted, it would be necessary to have knowledge of the crystallographic coordinates of the compounds, because as our experience has shown in the PCM calculations in metal-oxygen compounds, the electric-field gradient—and therefore β— is highly sensitive to uncertainties in the oxygen coordinates.

IV. CONCLUSIONS

We have studied by PAC the hyperfine interaction of ^{181}Ta in a Sn-O film prepared by thermal evaporation of Sn in a rare oxygen atmosphere.

We have done the hyperfine characterization of ^{181}Ta in the structures along the evolution of the film from the initial amorphous product up to the final sample oxidation and crystallization. Our PAC and CEMS results, throughout the experiment, are not in contradiction with an amorphicity due to positional disorder.

A tentative identification of the SnO hyperfine parameters is also made, although a definitive assignment is expected to derive only from experiments on pure SnO.

The unique SnO_2 phase is obtained after a crystallization process at 1373 K, making possible the identification of the hyperfine parameters of ^{181}Ta in SnO_2. The constancy of these parameters with changing temperature is in agreement with the *s* character of the conduction band.

Finally, the β factors obtained for ^{181}Ta in these oxides are in good agreement with those quoted by Bolse *et al.* for ^{111}In, who suggest that this parameter is mostly defined by the nearest-neighbor oxygen coordination and increases with the number of *NN* oxygen ions.

ACKNOWLEDGMENTS

The authors are indebted to Professor R. C. Mercader for very fruitful discussions and experimental supervision concerning CEMS measurements. This work was partially supported by the Consejo Nacional de Investigaciones Científicas y Técnicas (CONICET) and the Kernforschungzentrum Karlsruhe G.m.b.H, Germany. The support of the Deutscher Akademischer Austauschdienst is also appreciated.

[1]H. Haas and D. A. Shirley, J. Chem. Phys. **58**, 3339 (1973).
[2]J. Desimoni, A. G. Bibiloni, L. A. Mendoza Zélis, A. F. Pasquevich, F. H. Sánchez, and A. R. López García, Phys. Rev. B **28**, 5739 (1983); A. G. Bibiloni, J. Desimoni, C. P. Massolo, L. A. Mendoza Zélis, F. H. Sánchez, and A. R. López Garcia, Phys. Rev. B **29**, 1109 (1984).
[3]W. Bolse, M. Urhmacher, and K. P. Lieb, Mater. Sci. Eng. **69**, 375 (1985).
[4]Proceedings of the International Conference on Hyperfine Interactions, Bangalore, 1987 [Hyperfine Interact. **34**, 1 (1987)]; Proceedings of the International Conference on Hyperfine Interactions, Prague, 1989 [Hyperfine Interact. (to be published)].
[5]M. S. Moreno, A. G. Bibiloni, C. P. Massolo, J. Desimoni, and M. Renteria, Phys. Rev. B **40**, 2546 (1989).
[6]A. G. Bibiloni, J. Desimoni, C. P. Massolo, and M. Renteria, Phys. Rev. B **38**, 20 (1988).
[7]M. Renteria, A. Bartos, A. G. Bibiloni, M. Urhmacher, and K. P. Lieb (unpublished).
[8]G. S. Collins, T. Kachnowski, N. Benczer-Koller, and M. Pasternak, Phys. Rev. B **19**, 1369 (1979).
[9]T. Feng, A. K. Ghosh, and C. Fishman, J. Appl. Phys. **50**, 8070 (1979).
[10]M. H. Madhusudhana Reddy, S. R. Jawalekar, and A. N. Chandorkar, Thin Solid Films **169**, 117 (1989).
[11]J. Tafto, G. Rajeswaran, and P. E. Vanier, J. Appl. Phys. **60**, 602 (1986).
[12]J. J. Couderc, in *L'Ordre et le Désordre Dans Les Matériaux, Ecole d'Hiver—Aussois (1984),* edited by F. Reynaud, N. Clément, and J. J. Couderc (Les éditions de Physique, Les Ulis Cedex, 1984), p. 347.
[13]M. S. Moreno, J. Desimoni, R. C. Mercader, and A. G. Bibiloni (unpublished).
[14]M. Rentería, D. Wiarda, A. G. Bibiloni, and K. P. Lieb, Hyperfine Interact. (to be published).
[15]F. Requejo, A. G. Bibiloni, C. P. Massolo, M. Rentería, and J. Desimoni, Phys. Status Solidi A **116**, 937 (1989).
[16](a) W. Bolse, A. Bartos, J. Kesten, M. Uhrmacher, and K. P. Lieb (unpublished); (b) J. Kesten, W. Bolse, K. P. Lieb, and M. Uhrmacher, Hyperfine Interact. (to be published).
[17]W. Bolse, M. Uhrmacher, and J. Kesten, Hyperfine Interact. **35**, 981 (1987).
[18]A. F. Pasquevich, F. H. Sánchez, A. G. Bibiloni, J. Desimoni, and A. R. López García, Phys. Rev. B **27**, 963 (1983).
[19]L. A. Mendoza Zélis, A. G. Bibiloni, M. C. Caracoche, A. R. López García, J. A. Martínez, R. C. Mercader, and A. F. Pasquevich, Hyperfine Interact. **3**, 315 (1977).
[20]R. Summitt, J. A. Marley, and M. F. Borrelli, J. Phys. Chem. Solids **25**, 1465 (1964).
[21]R. M. Hazen and L. W. Finger, J. Phys. Chem. Solids **42**, 143 (1981).
[22]J. Pannetier and G. Denes, Acta Crystallogr. B **36**, 2763 (1980).
[23]R. W. G. Whycoff, *Crystal Structures* (Interscience, New York, 1965), Vol. 1, pp. 134 and 250.
[24]T. Butz and A. Lerf, Phys. Lett. **97A**, 217 (1983).
[25]M. C. Caracoche, T. M. Dova, A. R. López García, J. A. Martínez, and C. P. Rivas, Hyperfine Interact. **39**, 117 (1988).
[26]M. C. Caracoche, J. A. Martínez, C. P. Rivas, and A. R. López García, Hyperfine Interact. **23**, 221 (1985).
[27]C. J. Howard, R. J. Hill, and B. E. Reichert, Acta Crystallogr. B **44**, 116 (1988).
[28]R. Ruth and P. W. R. Corfield, J. Am. Ceram. Soc. **53**, 126 (1970).
[29]R. E. Hann, P. R. Suitch, and J. L. Pentecost, J. Am. Ceram. Soc. **68**, C-285 (1985).